

EUVE Observations of Clusters of Galaxies: M87

Thomas W. Berghöfer¹, Stuart Bowyer² and Eric Korpela²

¹ Max-Planck-Institut für extraterrestrische Physik, Giessenbachstraße, 85740 Garching, Germany

² Space Sciences Laboratory, University of California, Berkeley, CA 94720-7450, USA

Abstract. We present results of a re-analysis of archival EUVE data of the central region of the Virgo cluster. We employ the new analysis method developed by Bowyer, Berghöfer & Korpela (1999) and find diffuse emission reaching out to a distance of $\approx 13'$. The spatial distribution of this flux is incompatible with a thermal plasma origin. We investigate whether this emission is due to inverse Compton scattering of relativistic electrons against the 3° K black-body background. We show that this emission cannot be produced by an extrapolation to lower energies of the observed synchrotron radio emitting electrons and an additional component of low energy relativistic electrons is required.

1. Introduction

Observations with the *Extreme Ultraviolet Explorer* (EUVE) have provided evidence that a number of clusters of galaxies produce intense EUV emission. However, a variety of alternative explanations have been advanced which dismiss these results. Most recently, Arabadjis & Bregman (1999) argue that in some clusters the EUV excess can be explained away by a different cross section for absorption by hydrogen and helium in the foreground ISM column. Bowyer, Berghöfer & Korpela (1999) find that in some clusters this may explain some excess present in the ROSAT PSPC data, however, this cannot explain the intense EUV excesses reported with EUVE data.

Bowyer, Berghöfer & Korpela (1999) reexamined EUVE data of the clusters Abell 1795, Abell 2199, and Coma. They demonstrate that the initially reported results are based on an improper background subtraction. In previous analyses a flat background has been assumed. However, a detailed investigation of blank field observations with the EUVE Deep Survey (DS) instrument shows that the background consists of two independent components, a non-photonic background which is assumed to be constant over the entire detector field and a background due to photons. The non-photonic background level can be determined in obscured regions of the detector and can be directly subtracted from the raw data. However, the

photonic background is affected by telescope vignetting and must be treated differently.

In this paper we employ our new reduction method to EUVE archival data of the central part of the Virgo cluster. We compare our results with results derived from radio observations of this region. Finally, we consider the possibility that the observed diffuse EUV excess emission is due to an inverse Compton process of the known population of relativistic electrons in the ICM near M87.

2. Data and Data Analysis

The Virgo cluster has been observed for 36,000 s with the Deep Survey (DS) Telescope of EUVE (Bowyer & Malina, 1991). Data reduction was carried out with the EUVE package built in IRAF which is especially designed to process EUVE data.

In order to reduce the non-photonic (non-astronomical) background contribution to the scientific data we investigated the pulse-height spectrum of all detected events. A large number of EUVE DS observations of all kinds of astronomical targets has shown that a typical pulse-height spectrum consists of two components, a Gaussian profile representing the source events and an exponential background distribution. More details about the different background contributions to the DS data and the method of pulse-height thresholding can be found in Berghöfer et al. (1998). Here we screened out all events with pulse heights below 5300 ($\approx 15\%$ of the total) and above 13500 ($\approx 26\%$ of the total). From our experience with stellar and extragalactic observations with EUVE we know that this pulse-height selection effectively reduces the non-astronomical background in the data without any significant reduction of the source signal. The effect on the source signal is estimated to be lower than 4%.

Then we applied corrections for detector dead time and primbsching to the screened event list and produced a DS EUV image of the Virgo cluster. We then determined the remaining non-photonic background level in the image from highly obscured regions at the outer most parts of the field of view near the Lexan/B filter frame bars. This non-astronomical background contribution is assumed to be

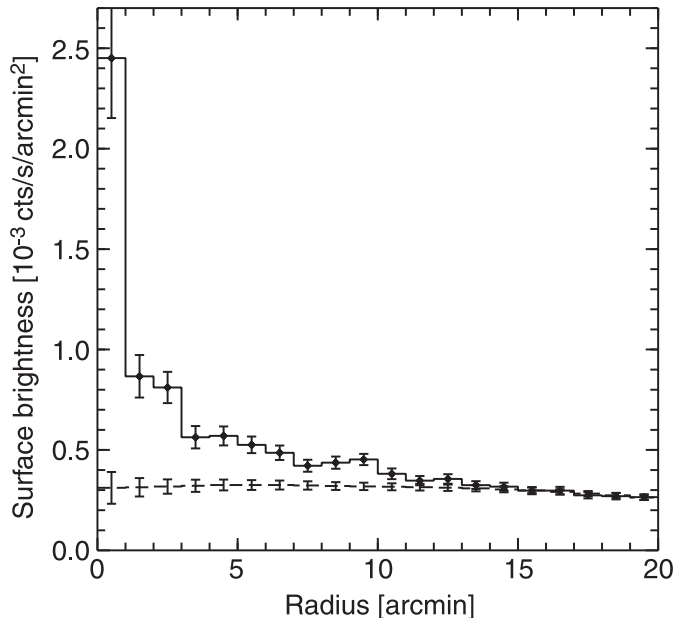


Fig. 1. The azimuthally averaged radial intensity profile of the EUV emission in the central part of Virgo (centered on M87) is shown as a solid line. The dashed line is the vignetted background. There is no EUV emission beyond $\approx 13'$.

constant over the entire detector field and was subtracted from the image.

In order to subtract the (vignetted) photonic background we computed the azimuthally averaged radial emission profile centered on M87. We used the EUVE DS sensitivity map provided by Bowyer, Berghöfer & Korpela (1999) to determine a radial sensitivity profile centered on the detector position of M87. This was the fit to the outer part (15–20') of the radial emission profile to determine the scaling factor between sensitivity profile and the photonic background in the data. The radial emission profile and the best fit background model are shown in Figure 1. The sensitivity map has been multiplied by the best fit scaling factor and subtracted from the DS image.

3. Results

Figure 1 demonstrates the presence of diffuse EUV emission in the vicinity of M87 which extends to a radius of $\approx 13'$. At larger radii the radial profile is well fit by the background model demonstrating the absence of any significant astrophysical signal. The initial publication on the diffuse EUV emission from Virgo (Lieu et al. 1996) claimed to detect excess emission to 20'.

In Figure 2 we plot the background subtracted radial EUV emission profile (solid line). The dashed line shows the expected EUV emission of the low energy tail of the X-ray emitting diffuse intracluster gas as derived in the following. Note that the inner 1' bin is dominated by the core and jet of M87 and must be ignored for the discussion of the diffuse emission. To determine the diffuse X-ray

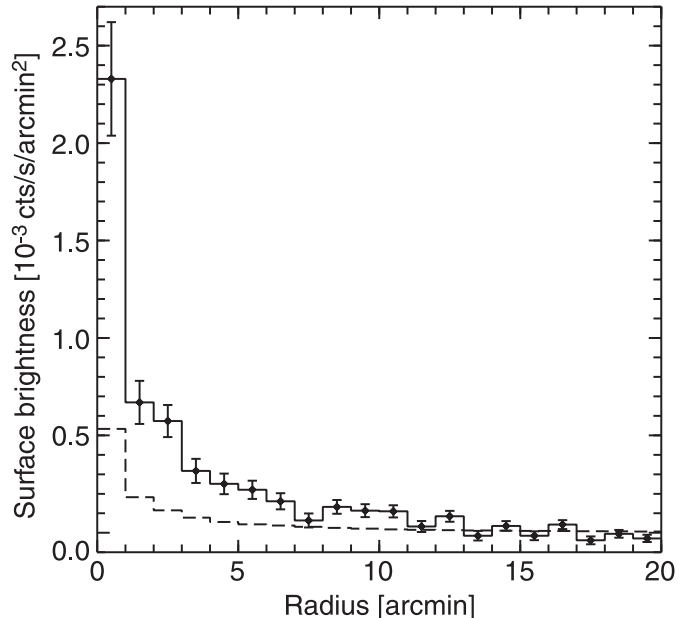


Fig. 2. The solid line shows the azimuthally averaged radial intensity profile of the background subtracted EUV emission in the central part of Virgo. The dashed line provides the contribution of the low energy tail of the X-ray emitting intracluster gas. The central 1' bin is dominated by the core and jet in M87 and must be ignored in the context of diffuse emission.

contribution to the observed EUV emission we processed ROSAT PSPC archival data of the Virgo cluster. We used standard procedures implemented in the EXSAS software package to produce an image from the photon event list. Then a vignetting corrected exposure map has been computed for this data set and a PSPC count rate image was generated by dividing the PSPC image by the exposure map.

We point out that the background in the ROSAT PSPC hard energy band is dominated by the photonic (vignetted) background and the contribution of the non-photonic background is minor. Therefore, a similar analysis as described for the EUVE DS data including a separation of the photonic and non-photonic background contributions is not essential. However, in the case of detectors with low effective areas (e.g., BeppoSAX), and less efficient rejection mechanisms for non-photonic events the background contribution must be treated separately.

For our analysis of the ROSAT PSPC data we selected only photon events in the hardest energy band, channels 90–236. This channel selection has several advantages: First, a contamination by a possible steep spectrum source at soft X-ray energies is excluded and, therefore, ensures that this band pass represents only thermal contributions to the overall diffuse emission in Virgo. Second, this part of the ROSAT band pass is almost unaffected by interstellar absorption. This minimizes errors due to possible differential ISM absorption effects when modeling theoretical conversion factors between DS and PSPC counts.

Third, the count rate conversion factor between DS and PSPC is almost temperature independent in the range of X-ray temperatures measured in the central Virgo region and, thus, ROSAT count rates of the diffuse X-ray emission can be converted into DS count rates by using one single conversion factor.

In order to be able to convert PSPC counts into DS counts we modeled conversion factors for a range of plasma temperatures (0.1–2.7 keV) employing the MEKAL plasma emission code with abundances of 0.34 solar (Hwang et al. 1997). These calculations include absorption by the interstellar medium. We used an ISM absorption column density of $1.72 \times 10^{20} \text{ cm}^{-2}$ (Hartmann & Burton 1997) and an absorption model including cross sections and ionization ratios for the ISM as described in Bowyer, Berghöfer & Korpela (1999). In Figure 3 we show the DS to PSPC conversion as a function of plasma temperature. As can be seen, for a wide range of temperatures (0.6–2.7 keV) the model conversion factor is constant within 15%. According to Böhringer et al. (1995) and Böhringer (1999), the temperature of the X-ray emitting intracluster gas in the Virgo cluster is ≈ 2 keV. In addition to this thermal gas component these authors detected several diffuse emission features near M87 which are significantly softer than the average Virgo cluster gas temperature. However, spectral fits to the ROSAT data do not provide temperatures below 1 keV (Böhringer, private communication). For temperatures near 1 keV the modeled conversion factor for a thermal gas is slightly lower than for higher temperatures. Therefore, the contribution of the lower temperature components to the overall diffuse X-ray emission in the EUV band pass is lower than the dominant 2 keV cluster gas component. Using the conversion factor appropriate for the mean cluster gas temperature of 2 keV for the entire emission including the softer thermal enhancements, slightly overestimates the low energy X-ray contribution to the EUV emission.

In Figure 4 we show the observed ratio between azimuthally averaged radial intensity profiles observed with the EUVE DS and PSPC. Within the error bars the ratio is constant (reduced $\chi^2 = 0.9$). The best fit value is 0.0186. The ratio for the inner 1' bin is consistent with this value, however, we excluded this due to the presence of emission from the core and jet of M87. Sarazin & Lieu (1998) have suggested that an increasing EUV to X-ray emission ratio towards larger distances from the cluster center is an indication of an inverse Compton process producing the EUV emission in the cluster. However, Figure 4 demonstrates that this is not observed in the central Virgo region.

On the other hand, our best fit value of 0.0186 is ≈ 4.3 times larger than expected for the low energy tail of the X-ray emitting gas in the Virgo cluster. Therefore, the X-ray contribution to the observed EUV excess in the central part of the Virgo cluster must be minor.

It is clear that the ratio between observed EUV flux and modeled X-ray contribution cannot directly be used to

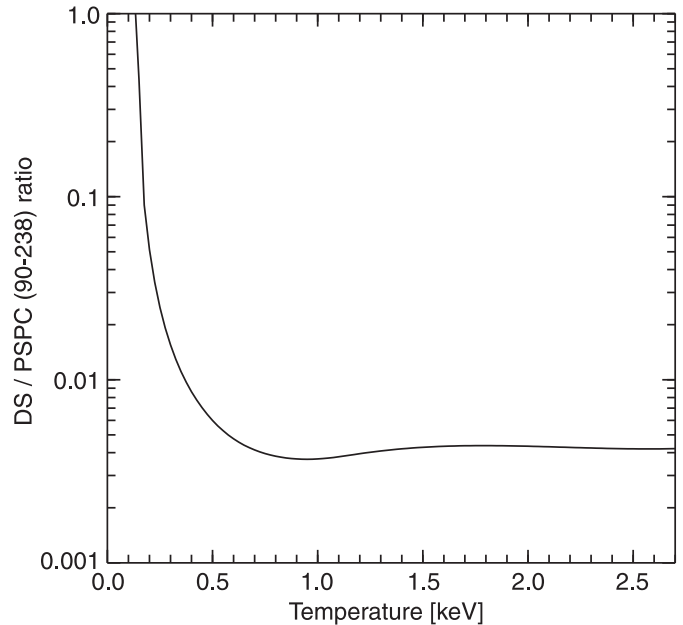


Fig. 3. Modeled conversion factors from ROSAT PSPC count rates into EUVE DS rates for a thermal plasma model including the ISM absorption towards the Virgo cluster.

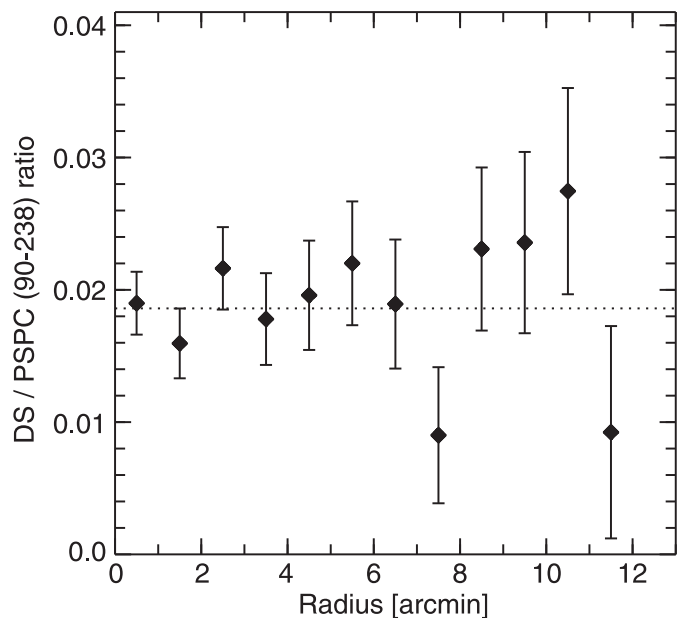


Fig. 4. The ratio between observed azimuthally averaged intensity profiles observed with the EUVE DS and ROSAT PSPC. The dotted line represents the best fit value of 0.0186 assuming a constant ratio.

determine the physical parameters of the source. Instead, one must first subtract the X-ray contribution from the observed EUV emission.

In Figure 5 we show the spatial distribution of the EUV excess emission in the central Virgo region; the background and the contribution of the low energy tail of the X-ray emitting ICM have been subtracted. The central

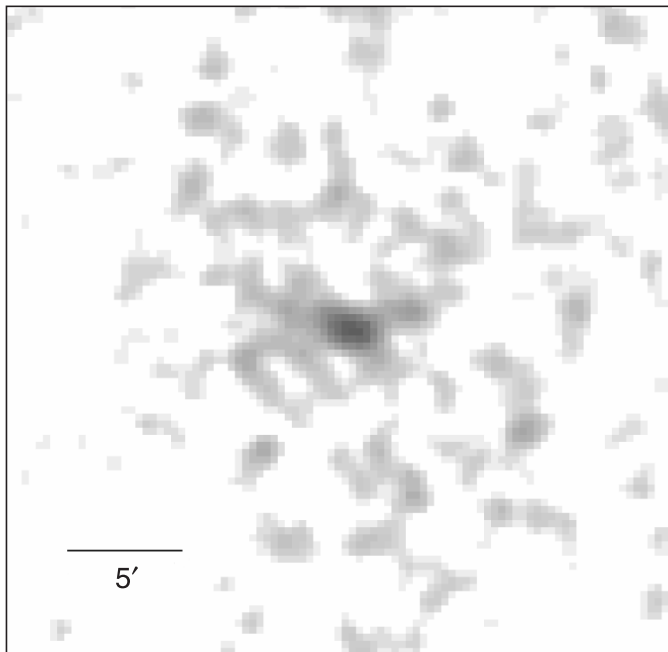


Fig. 5. Spatial distribution of the EUV excess emission in the central Virgo region. The contribution of the low energy tail of the X-ray emitting ICM has been subtracted from the data.

emission peak at the position of M87 is surrounded by a diffuse EUV emission structure which is asymmetric in shape. Its extent varies between $1'$ and $7'$. Several arm-like features are visible. At larger radii the EUV emission results from a number of apparently discrete and extended diffuse features in the M87 radio halo. These emission features are consistent with the emission seen in the surface brightness profile (Figure 2) between 9 – $13'$. These asymmetric features show the flux is not produced by a gravitationally bound thermal gas.

4. Discussion and Conclusions

The results of our reanalysis show a clear EUV excess in the central Virgo region around M87. Compared to previous studies the extent of this emission is smaller and extends only to $\approx 13'$ from the center of M87.

To further explore the spatial distribution of the EUV excess we compare this emission to a 90 cm radio map of the central Virgo region near M87 (Owen, Eilek & Kasim 1999). If the diffuse EUV emission is due to an inverse Compton process in the ICM one might expect to see similar emission features in both the EUV and radio image. In Figure 6 we show a contour plot of the EUV emission superposed on the 90 cm radio map. As can be seen, the EUV emission peaks at the position of the radio emission of the core and jet of M87. EUV excess emission features are, however not directly coincident with any of the other brighter features visible in the radio map. The EUV emission is also not associated with the X-ray emission features seen in the ROSAT PSPC images in excess of the wide dif-

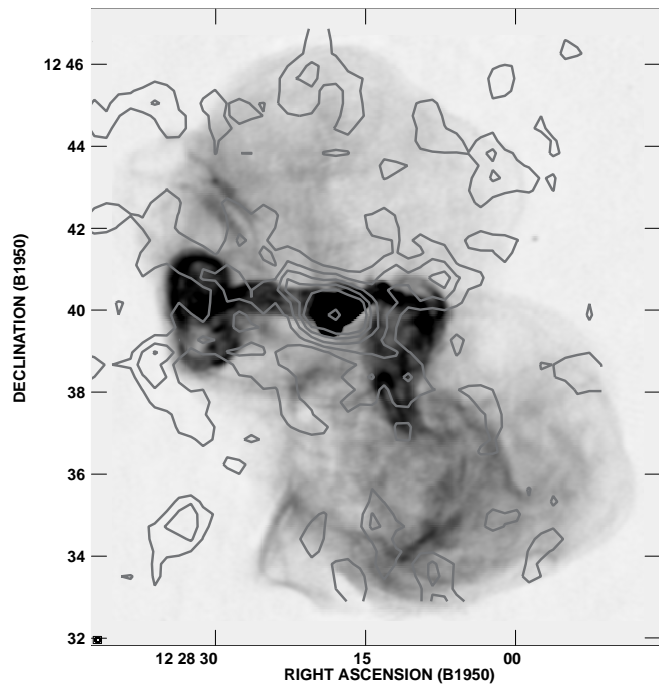


Fig. 6. Contour plot of the background and X-ray subtracted EUV emission shown superposed on the 90 cm radio map of the M87 halo. The contours provide fluxes of 1.5, 4.5, 7, 10, 13, and 27σ above the noise level.

fuse ICM gas component in Virgo (cf. Böhringer 1999 and Harris 1999).

We now investigate whether the integrated flux of the diffuse EUV emission is compatible with an inverse Compton origin of the observed EUV excess in the central Virgo region. We have used the observed radio synchrotron power law spectrum of the M87 halo ($\alpha = 0.84$, Herbig & Readhead 1992) to compute the underlying distribution of relativistic electrons in this region and its inverse Compton flux. Note that the radio spectrum needs to be extrapolated into the low frequency range near 1 MHz which is not observable due to ionospheric effects. The conversion from the synchrotron spectrum into an electron energy distribution depends on the average magnetic field strength in the ICM and hence we can derive a relation between magnetic field strength and the inverse Compton flux produced by the relativistic electrons. Figure 7 shows the result. The flux is folded with the EUVE DS response and given in units of DS counts/s which allows a direct comparison to the observed integrated DS count rate of the diffuse emission (horizontal line in Figure 7). As can be seen, for a magnetic field strength of $\approx 3 \mu\text{G}$ the observed flux matches the model flux. Note

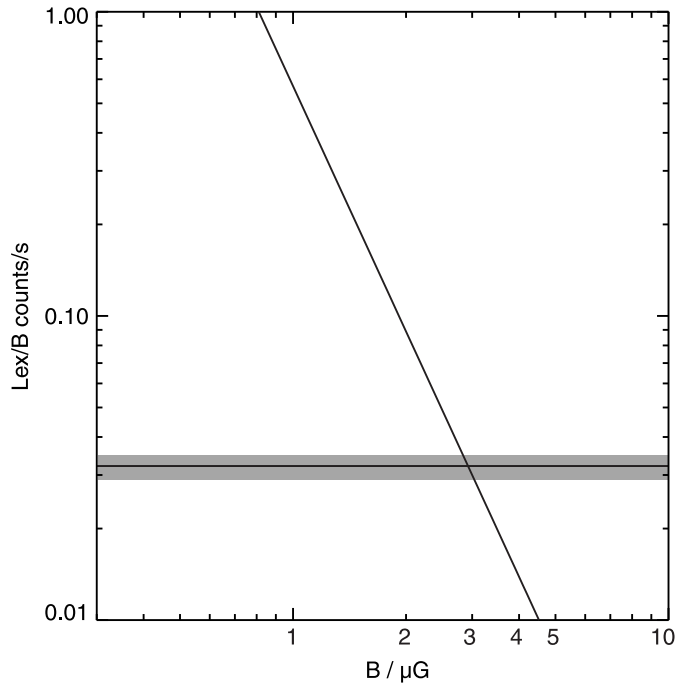


Fig. 7. EUVE DS count rate as a function of magnetic field strength. The horizontal line provides the observed total count rate for the diffuse emission component. The error in this value is shown as a gray shaded area.

that this value would also be consistent with Faraday rotation measurements in the M87 halo (Dennison 1980).

However, with $\alpha = 0.84$ the radio synchrotron spectrum is inconsistent with the required steep EUV to X-ray power law spectrum. In order to explain the observed EUV flux and the upper limit in the ROSAT PSPC hard band (channels 90–238) by a non-thermal power law type spectrum source we find a power law photon number index of $\alpha \geq 3.2$. Therefore, inverse Compton emission from the known population of relativistic electrons in the M87 halo cannot account for the observed EUV excess in the central Virgo region.

5. Summary

The observed EUV excess in the central Virgo region is not spatially consistent with either the distribution of the radio emission or the observed thermal X-ray excess emission seen in the ROSAT images. Due to the required steep EUV to X-ray spectrum this emission cannot be produced by an extrapolation to lower energies of the observed synchrotron radio emitting electrons. Therefore, as is the case in the EUV excess in the Coma cluster (cf. Bowyer & Berghöfer 1998), a second unknown population of relativistic electrons would be required to explain the observed EUV excess by inverse Compton's emission, if this were the underlying source mechanism.

Acknowledgements. We thank Jean Eilek for providing us a postscript file of the M87 radio map. We acknowledge useful discussions with John Vallerga, and Jean Dupuis. This work was supported in part by NASA contract NAS 5-30180. TWB was supported in part by a Feodor-Lynen Fellowship of the Alexander-von-Humboldt-Stiftung. SB and EK have been supported by EUVE.

References

- [1] Arabadjis, J. S. & Bregman J. N., 1999, *ApJ*, 514, 607
- [2] Berghöfer, T. W., Bowyer, S., Lieu, R., & Knude, J. 1998, *ApJ*, 500, 838
- [3] Böhringer, H., Nulsen, P. E. J., Braun, R. & Fabian, A. C. 1995, *MNRAS*, 274, L67
- [4] Böhringer, H. 1999, this workshop
- [5] Bowyer, S., & Malina, R. F. 1991, in *Extreme Ultraviolet Astronomy*, ed. R. F. Malina & S. Bowyer (New York: Pergamon), 397
- [6] Bowyer, S., & Berghöfer, T. W. 1998, *ApJ*, 506, 502
- [7] Bowyer, S., Berghöfer, T. W. & Korpela, E. 1999, this workshop
- [8] Dennison, B. 1980, *ApJ*, 236, 761
- [9] Harris, D. 1999, this workshop
- [10] Hartmann, D., & Burton, W. B. 1997, *Atlas of Galactic Neutral Hydrogen* (Cambridge: Cambridge Univ. Press)
- [11] Herbig, T., & Readhead, A. C. S. 1992, *ApJS* 81, 83
- [12] Hwang, U., Mushotzky, R. F., Loewenstein, M., Markert, T. H., Fukazawa, Y. & Matsumoto, H. 1997, *ApJ*, 476, 560
- [13] Lieu, R., Mittaz, J., Bowyer, S., et al. 1996, *ApJ*, 458, L5
- [14] Owen, F., Eilek, J. & Kassim, N., 1999, in prep.
- [15] Sarazin, C., & Lieu, R. 1998, *ApJ*, 494, L177